Supplementary materials for

Direct observation of double-layered reaction intermediates at the atomic scale during methane pyrolysis

Hui Wang[1,4]*, Yongli Shen[1,4], Shengnan Yue[1], Shanshan Liu[1], Lin Gu[1], Wenjuan Yuan[1], Chao Zhang[1], Yu Huang[2], Xiangfeng Duan[2], Wei Xi[1,3]*, Tong-Bu Lu[1,]*

[1]Tianjin Key Lab of Advanced Functional Porous Materials, Institute for New Energy Materials and Low Carbon Technologies, School of Materials Science and Engineering, Tianjin University of Technology, Tianjin, 300384, China.

[2]Department of Chemistry and Biochemistry, University of California, Los Angeles, CA, USA.

[3]School of Chemical Engineering & Technology, Tianjin University, Tianjin 300350, China.

[4]These authors contributed equally: Hui Wang, Yongli Shen.

*Corresponding author. E-mail address: wanghui2020@email.tjut.edu.cn, xiwei@tjut.edu.cn, lutongbu@tjut.edu.cn

Contents

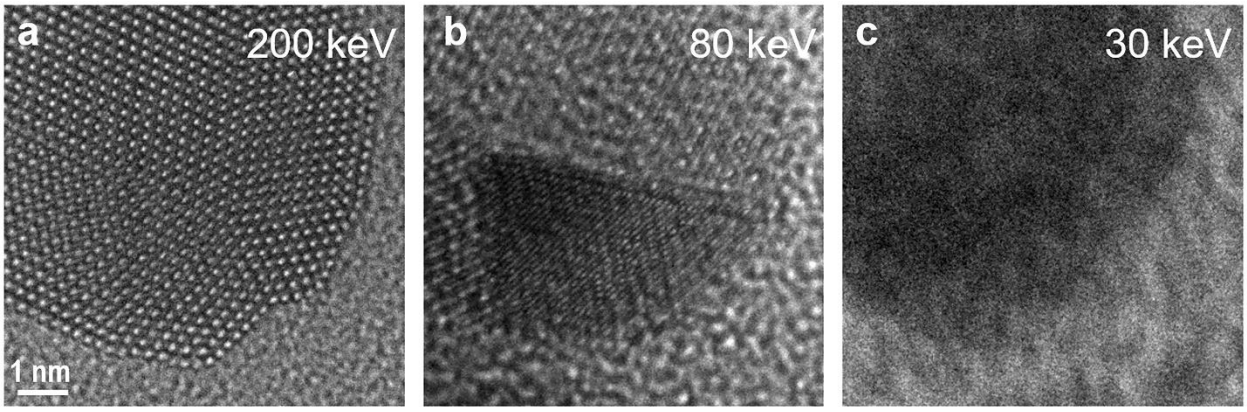

Supplementary Fig. 1 | TEM images of NPG with different accelerating voltages. a, 200, **b,** 80 and **c,** 30 keV.

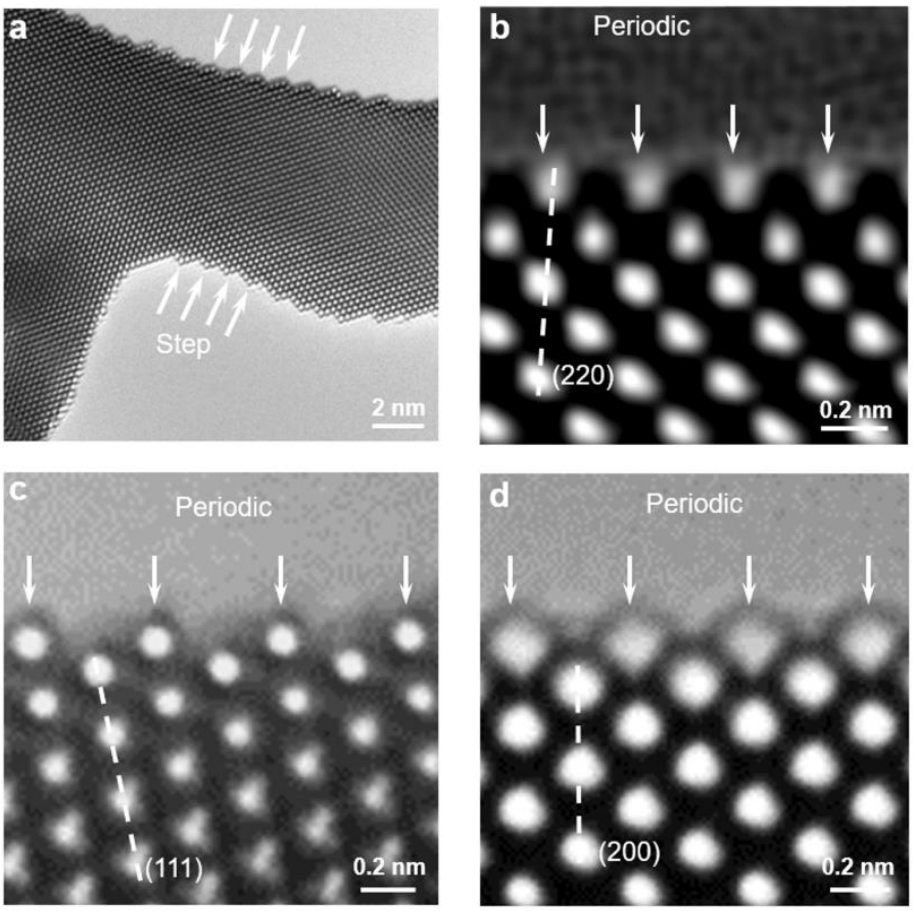

Supplementary Fig. 2 | Periodic structures on the surface of NPG sample. a, Zigzag and **b, c, d,** periodic structures of fresh NPG under vacuum conditions observed by aberration-corrected objective TEM. The periodic structures are indicated with white arrows.

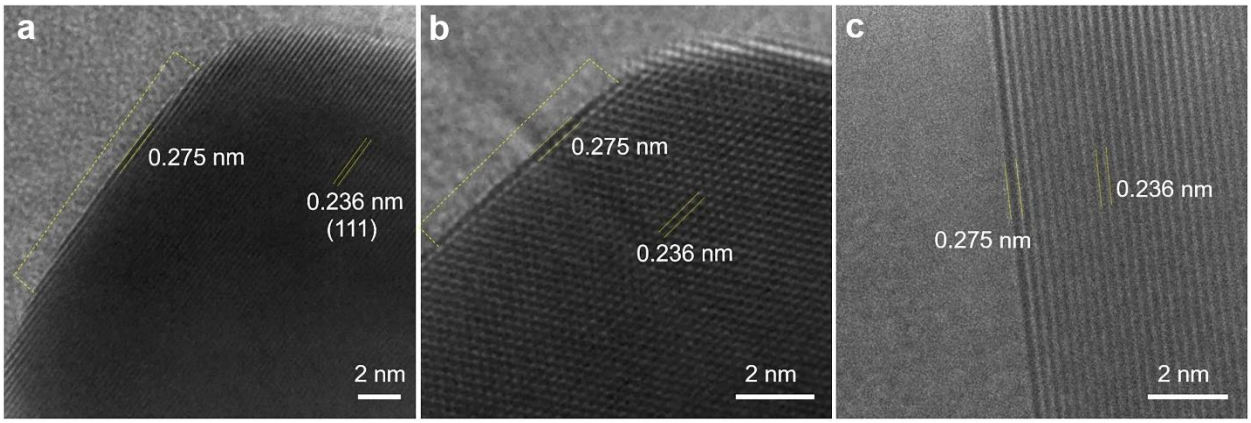

Supplementary Fig. 3 | The expansion of the outermost layer during CH_4 pyrolysis reaction. **a–c,** Three different regions with the outermost layer spacing expanded to 0.275 nm during CH_4 pyrolysis, while the interior counterparts remained as 0.236 nm. Some faint intermediate adsorbates on the outermost layer of NPG could be seen in (**a**) and (**b**), as indicated with the dashed yellow boxes.

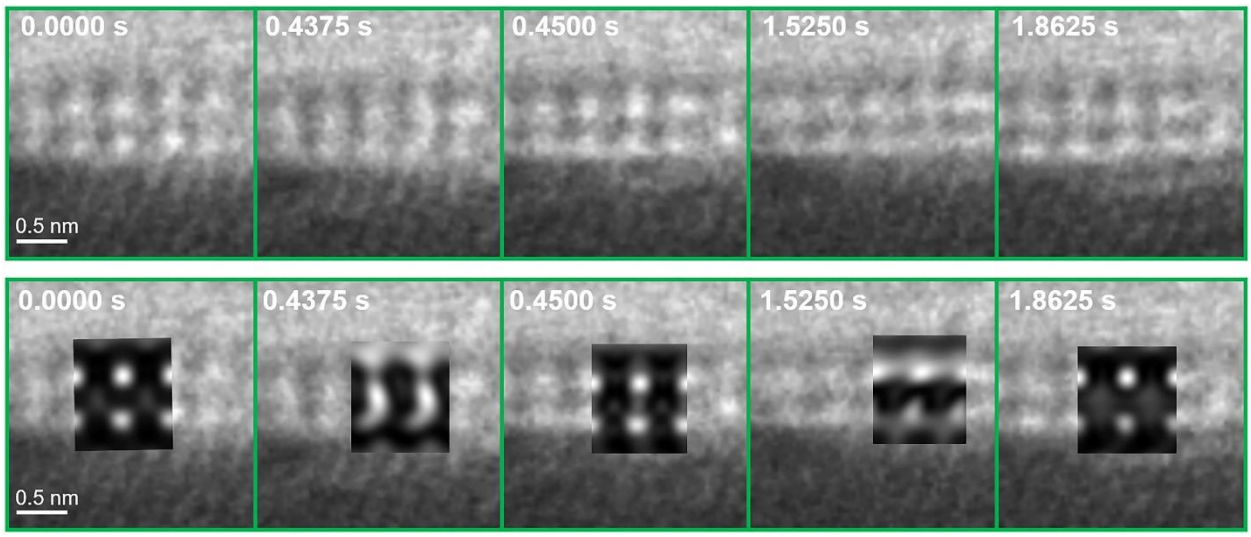

Supplementary Fig. 4 | HRTEM images (top) and the corresponding simulation (bottom) of the evolved double-layered adsorption structure in Fig. 3a. The simulation results (bottom) show a very similar contrast to the adsorption structure, compatible with the HRTEM image.

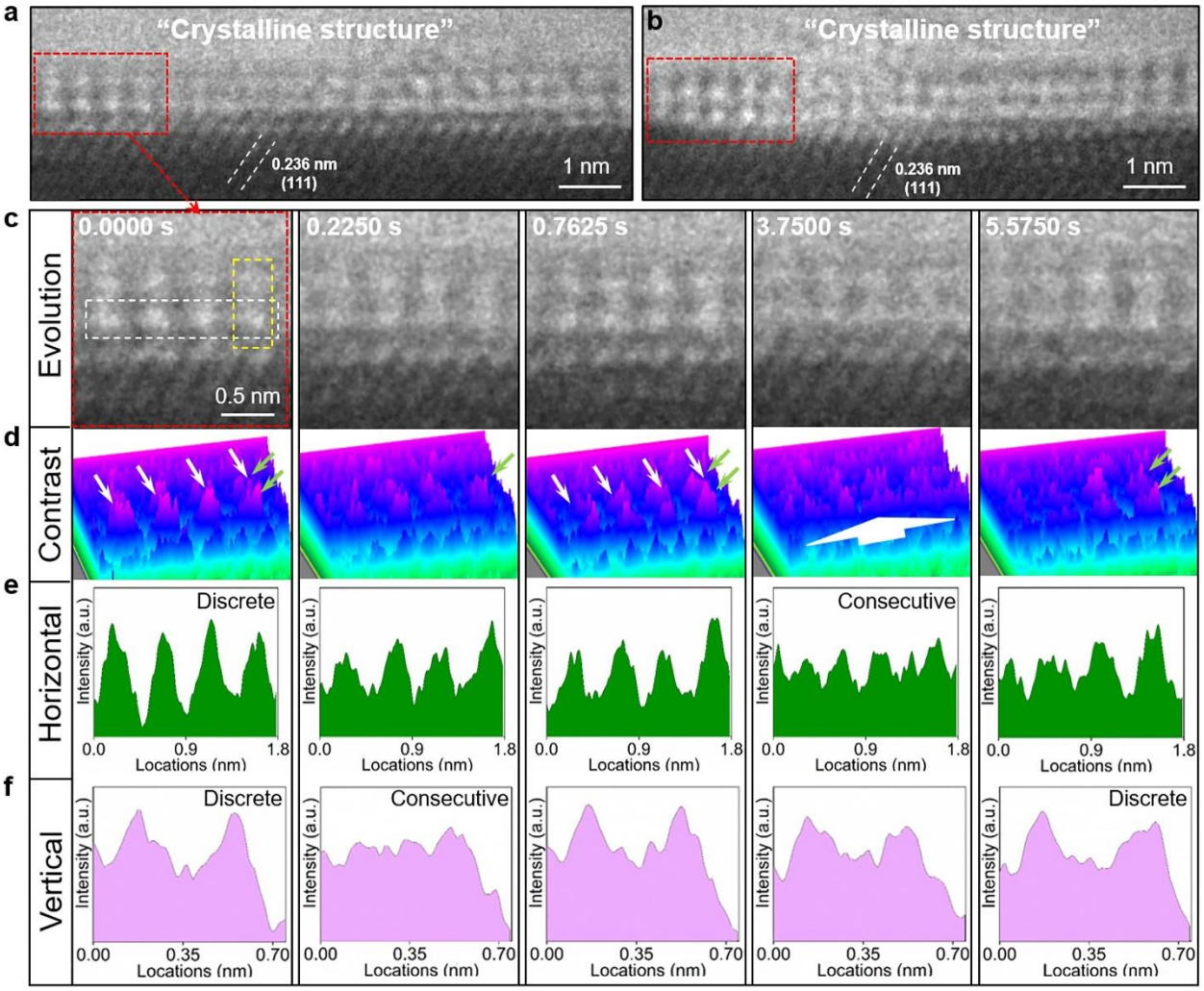

Supplementary Fig. 5 | The "crystalline structure" evolution at the edge of Au(111) planes. **a, b** Typical images of crystalline structure with discrete atom columns in the red dashed boxes. The detailed evolution process for (**b**) was shown in Fig. 3. **c**, The evolution process of a typical crystalline structure with discrete atom columns in (**a**). **d,** The entire contrast analysis corresponds to the evolution images in (**c**). **e,** Contrast analysis for the horizontal atom columns during evolution indicated by white dashed boxes in (**c**). **f,** Contrast analysis for the vertical atom columns during evolution indicated by yellow dashed boxes in (**c**). Evidently, the horizontal row of atom columns became consecutive at 3.7500 s, while the vertical pair had already reversed to consecutive state at 0.2250 s. This clearly shows that the adsorption structures are dynamic and can easily evolve into different morphologies, while they are essentially the same.

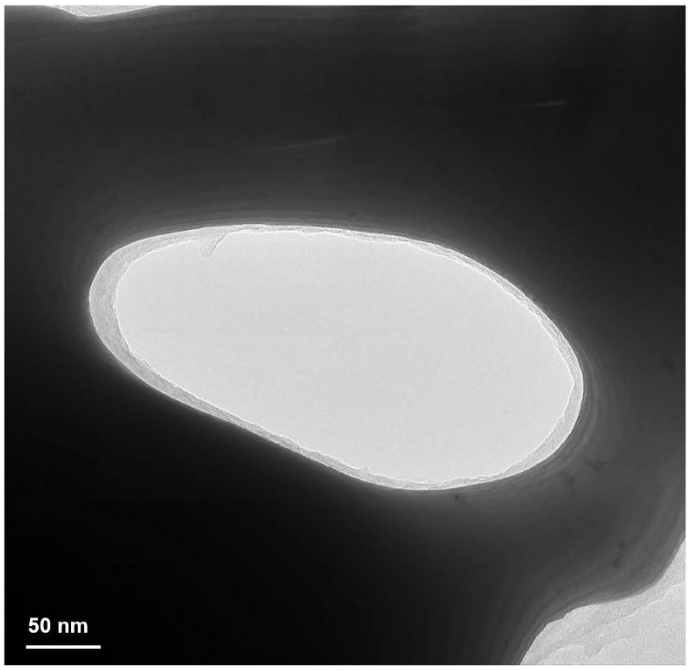

Supplementary Fig. 6 | Adsorbates and amorphous carbon distributed throughout the entire pore of the NPG.

5

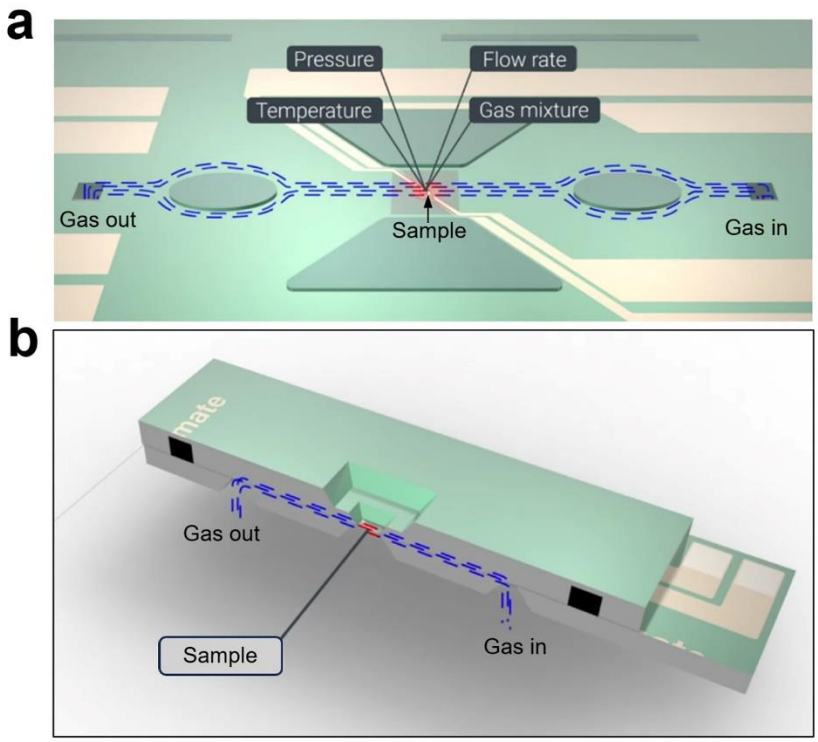

Supplementary Fig. 7 | The flowing system of the sample chip used for *in situ* observation. Observations from **(a)** quasi-top view and **(b)** quasi-lateral view perspective. (Adapted with the permission from DENSsolutions)

5

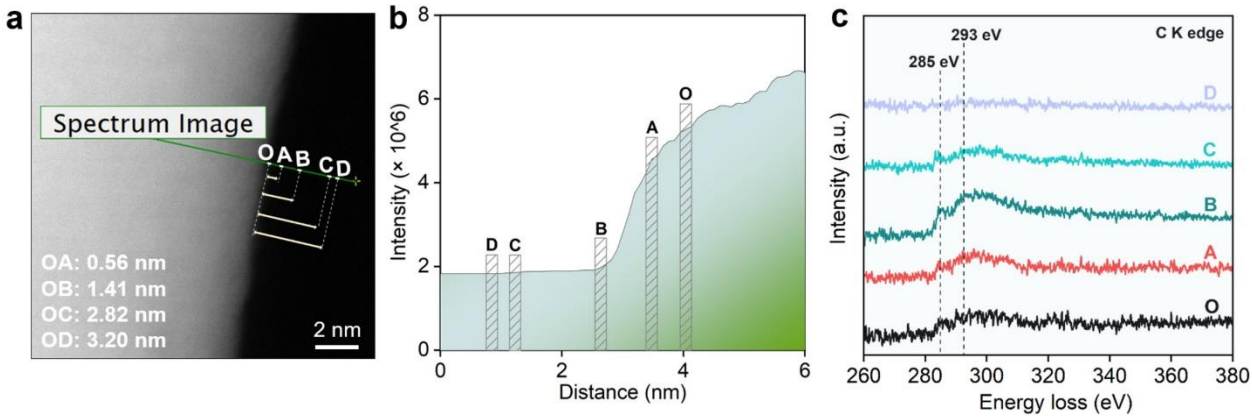

Supplementary Fig. 8 | EELS analysis of the adsorbates at certain NPG edge with more carbon generation. a, Position and distance marker for different points on annular dark-field image. **b,** Contrast analysis along the green line in **(a)**. **c,** EELS spectra comparison at different points. The OA distance of 0.56 nm approximates to the height of the double-layered adsorbates at the edge of Au(111) plane (0.58 nm, measured on *in situ* TEM image).

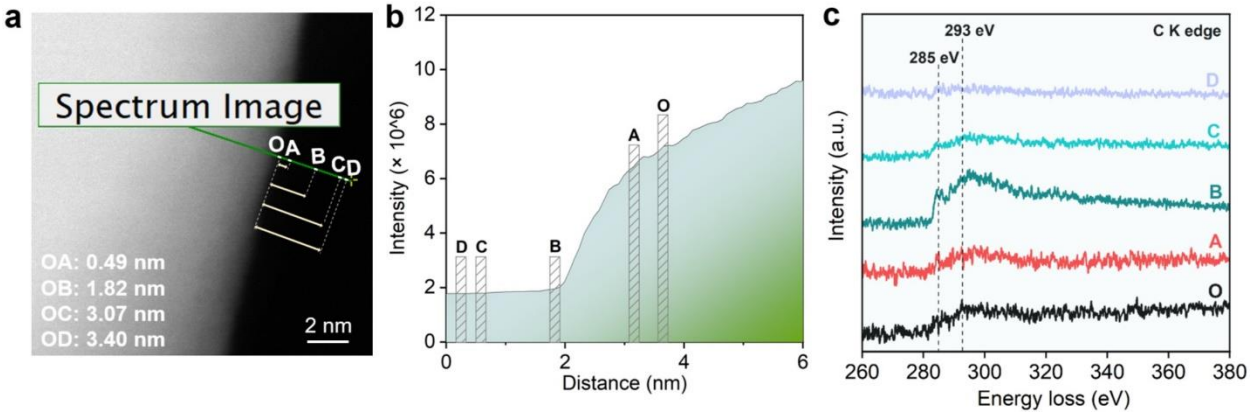

Supplementary Fig. 9 | EELS analysis of the adsorbates at another NPG edge with more carbon generation. a, Position and distance marker for different points on annular dark-field image. **b,** Contrast analysis along the green line in (**a**). **c,** EELS spectra comparison at different points. The OA distance of 0.49 nm approximates to the height of the double-layered adsorbates at the edge of Au(220) plane (0.51 nm, measured on *in situ* TEM image).

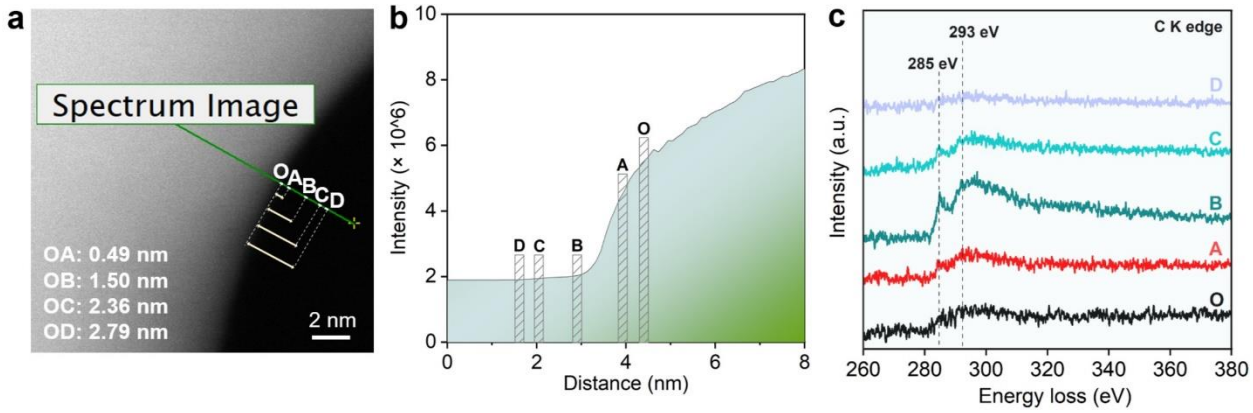

Supplementary Fig. 10 | EELS analysis of the adsorbates at another NPG edge with more carbon generation. a, Position and distance marker for different points on annular dark-field image. **b,** Contrast analysis along the green line in (**a**)**. c,** EELS spectra comparison at different points. The OA distance of 0.49 nm approximates to the height of the double-layered adsorbates at the edge of Au(220) plane (0.51 nm, measured on *in situ* TEM image).

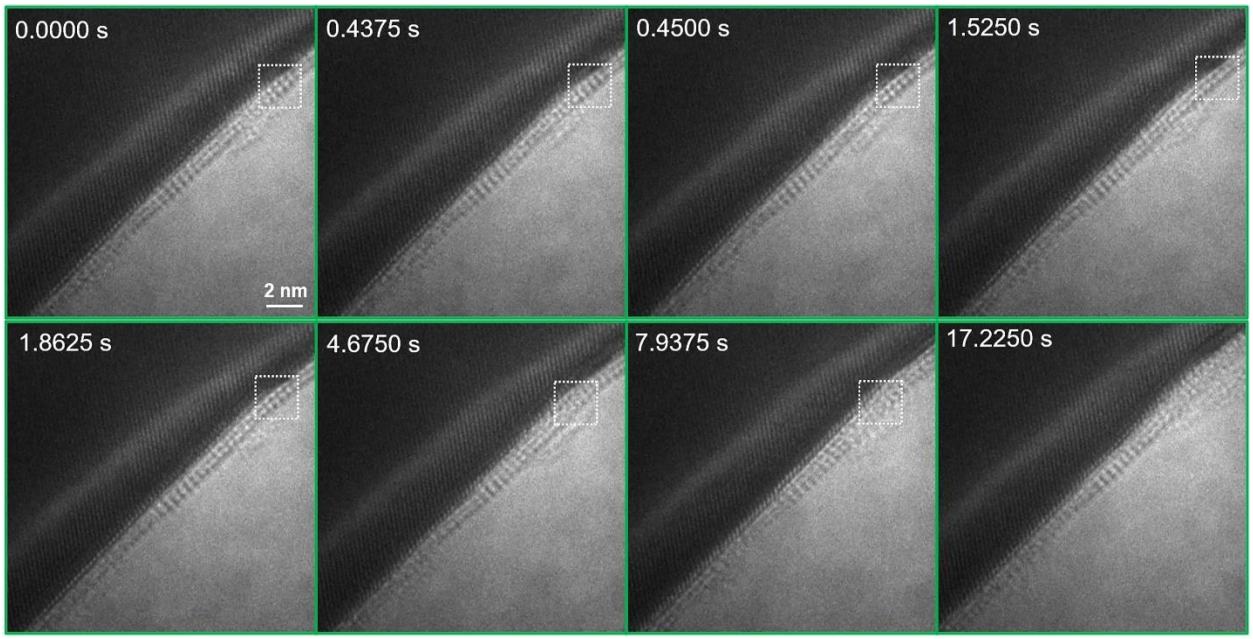

Supplementary Fig. 11 | The dynamic evolution of the double-layered adsorption structure following Fig. 3. The double-layered adsorption structure was labelled with white dashed box. It became obscured by amorphous carbon at 4.6750 s and was no longer visible at 17.2250 s

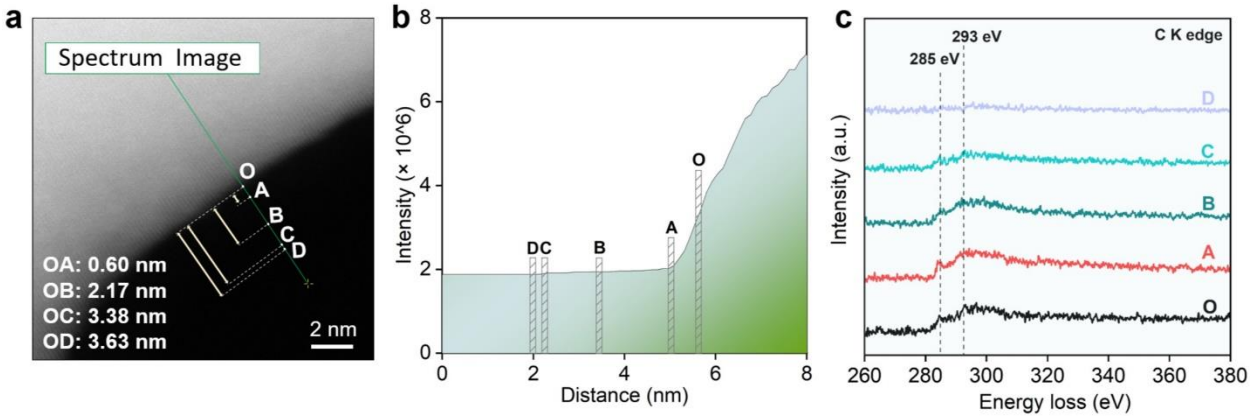

Supplementary Fig. 12 | EELS analysis of the adsorbates at certain NPG edge with less carbon generation. a, Position and distance marker for different points on annular dark-field image. **b,** Contrast analysis along the green line in **(a)**. **c,** EELS spectra comparison at different points. The OA distance of 0.60 nm approximates to the height of the double-layered adsorbates at the edge of Au(111) plane (0.58 nm, measured on *in situ* TEM image).

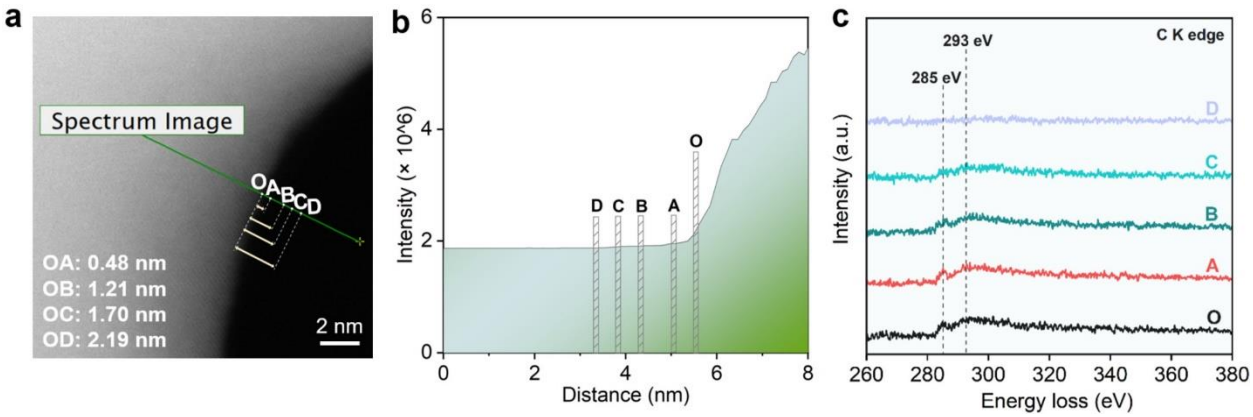

Supplementary Fig. 13 | EELS analysis of the adsorbates at another NPG edge with less carbon generation. a, Position and distance marker for different points on annular dark-field image. **b,** Contrast analysis along the green line in (**a**)**. c,** EELS spectra comparison at different points. The OA distance of 0.48 nm approximates to the height of the double-layered adsorbates at the edge of Au(220) plane (0.51 nm, measured on *in situ* TEM image).

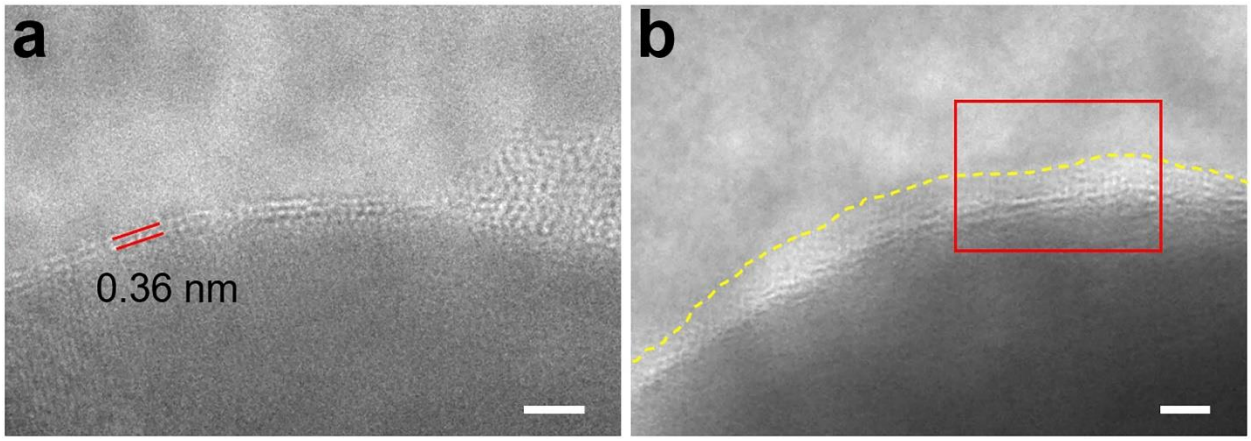

Supplementary Fig. 14 | The adsorbates comparison at high and low temperatures. The *in situ* observations at (**a**) 350 °C and (**b**) 30 °C. The scale bar is 2 nm. The double-layered structure is relatively distinct at 350 °C. It became blurry but retained in a small region when cooled down to 30 °C.

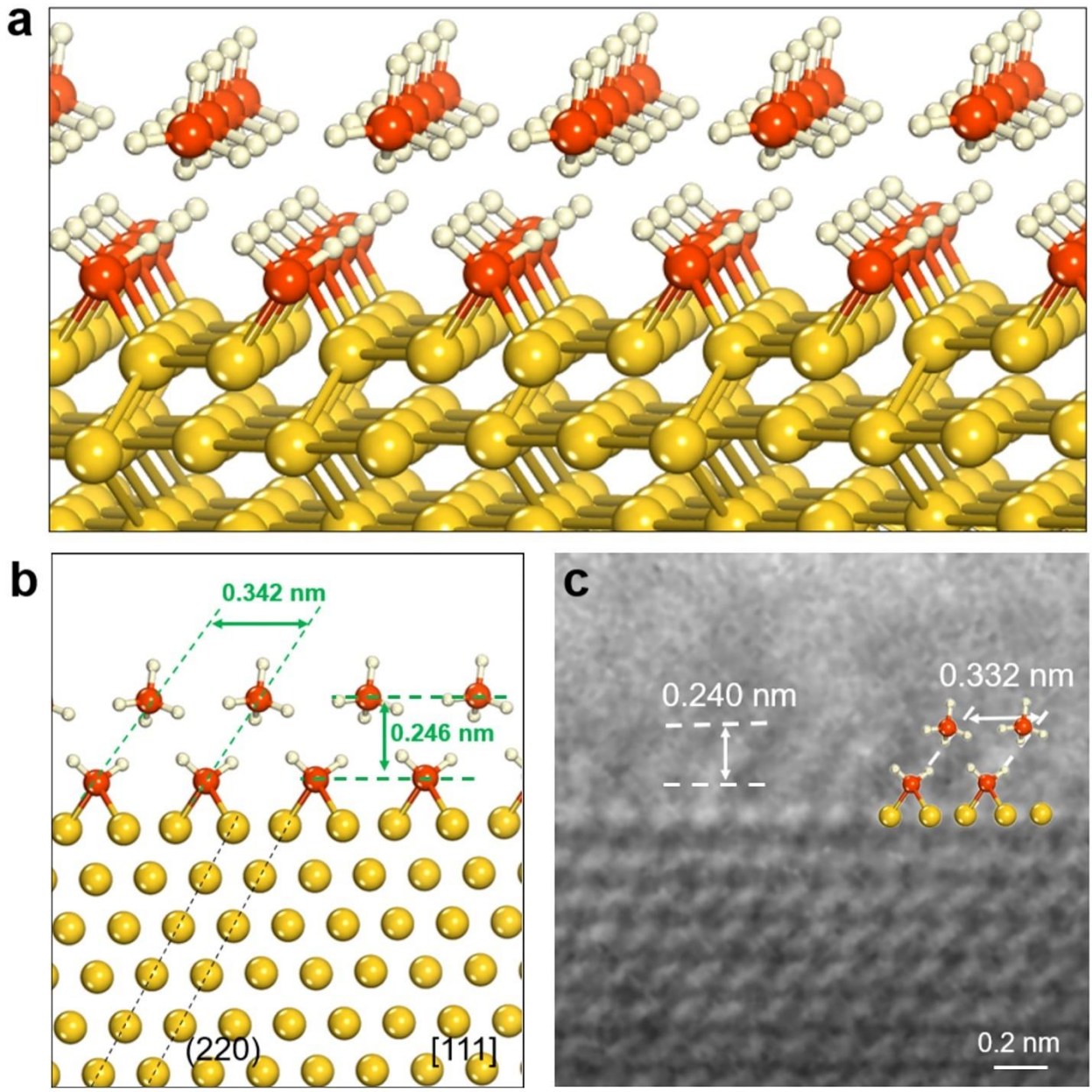

Supplementary Fig. 15 | Structure comparison for simulated reaction intermediate adsorption structure and the observed adsorption at the flat edge of Au(220) plane with flat periodic sites. a, The optimized stereoscopic structure for reaction intermediates adsorbing on the edge of Au(220) plane. **b,** The side view of Au(220) plane observed along the <111> direction for the stereoscopic structure in (**a**). **c,** A typical TEM image with the horizontal and vertical spacings of the adsorption structure labeled. These spacings are in good agreement with the theoretical values in (**b**).

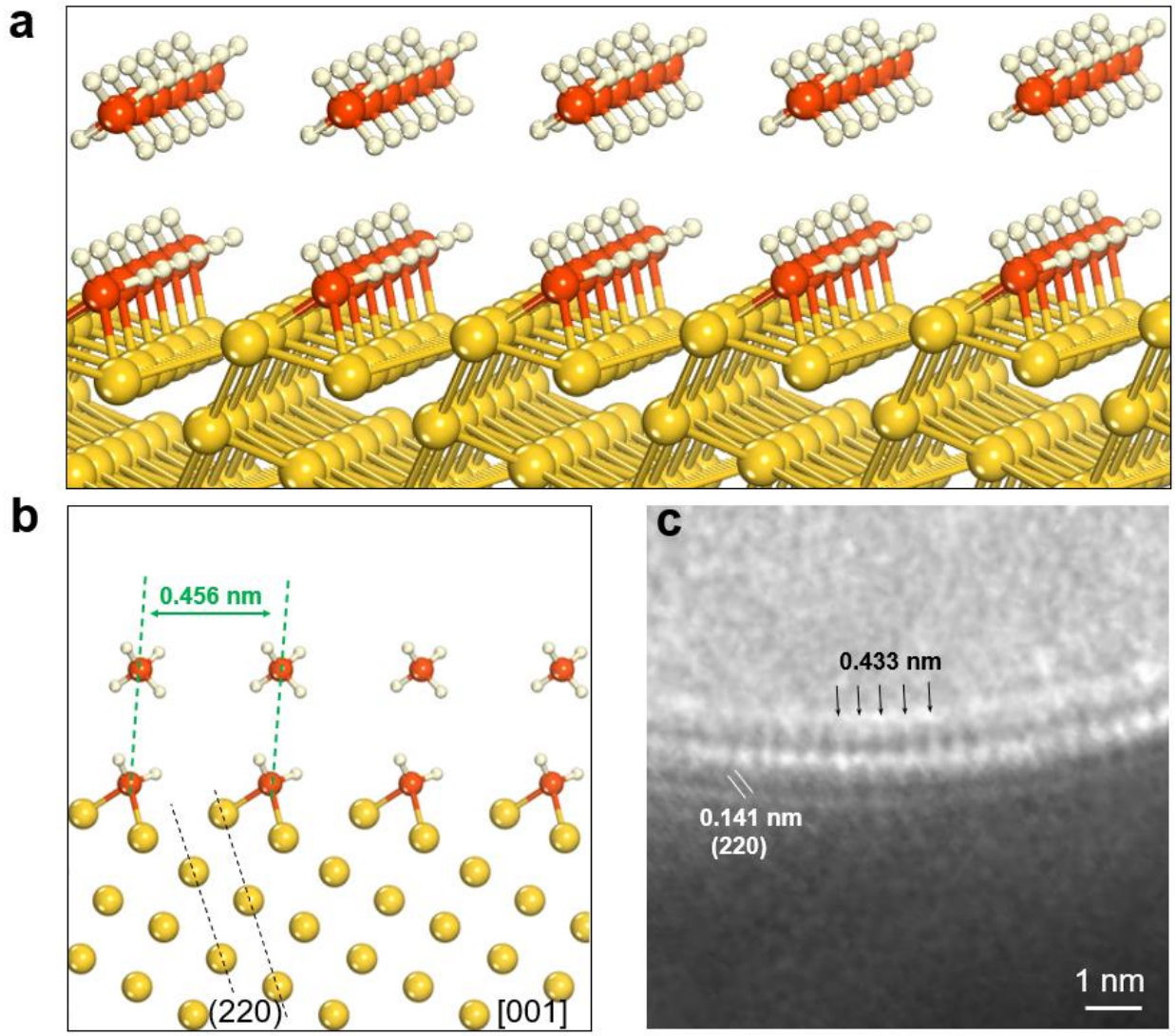

Supplementary Fig. 16 | Structure comparison for simulated reaction intermediate adsorption structure and the observed adsorption at the periodic stepped edge of Au(220) plane. a, The optimized stereoscopic structure for reaction intermediates adsorbing on the edge of Au(220) plane. **b,** The side view observed along the <001> direction of the stereoscopic structure in (**a**). The comb-teeth spacing was specified. **c,** A typical TEM image with the horizontal spacing of the adsorption structure labeled. These spacings are in good agreement with the theoretical values in (**b**).

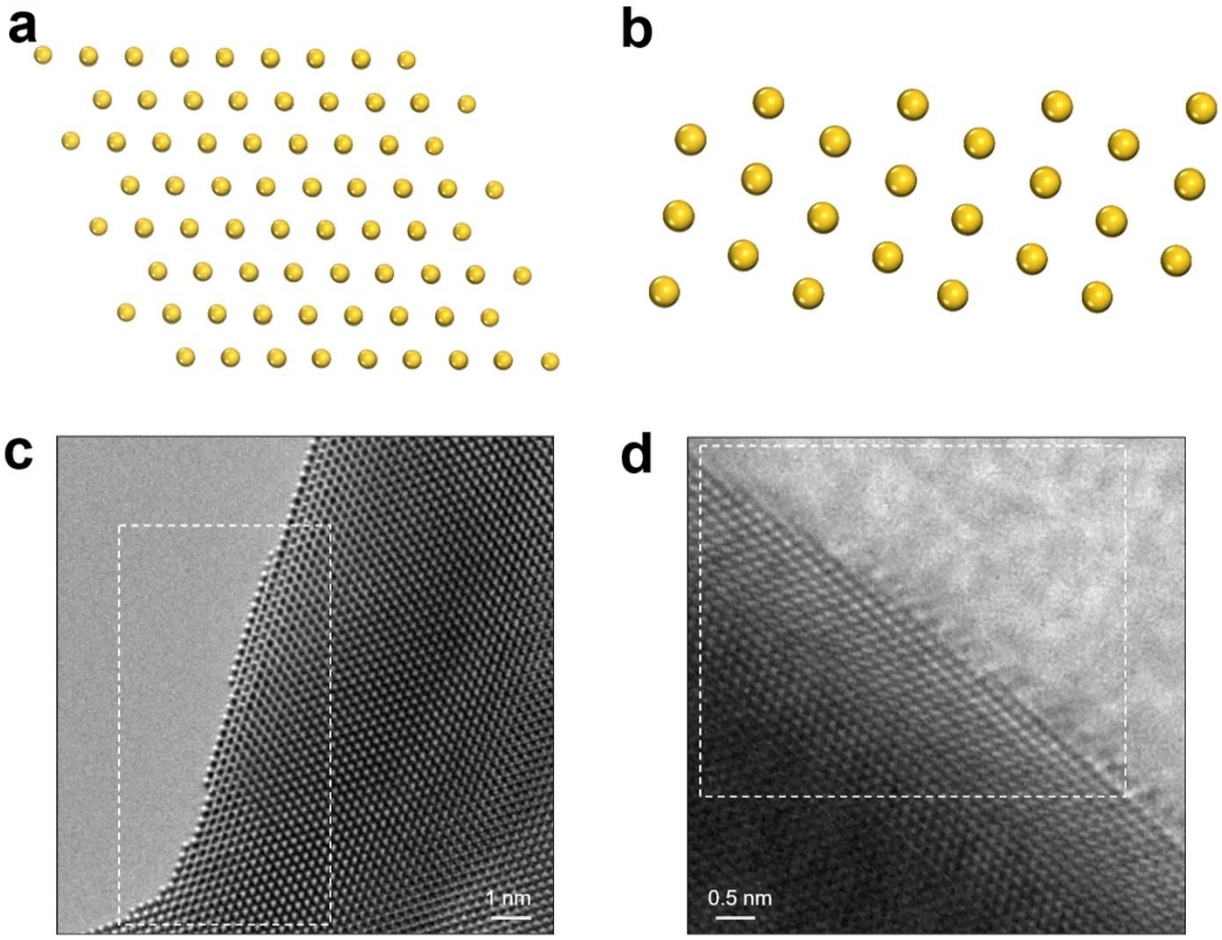

Supplementary Fig. 17 | Comparison of the DFT model and the actual NPG surface. a, The top and (**b**)**,** the side view of DFT optimized Au(111) surface. The actual NPG surfaces with discontinuous outermost layer Au atoms in (**c**) under vacuum conditions (no adsorbates) and in (**d**) during the reaction (with adsorbates). The discontinuous Au surfaces were labeled with white dashed boxes.

As displayed in Supplementary Fig. 17a and b, the DFT optimized Au surface maintains crystallographic integrity and periodicity, even under the theoretically infinite lattice expansion conditions. However, the actual NPG surface intrinsically lacks long-range structural uniformity, instead retaining only short-range periodicity even with adsorbates on it (Supplementary Fig. 17c, d). The outermost layer of NPG is composed of several Au atoms. When the second and the third layers are exposed to the outermost, they become the new outermost layer. Therefore, we think the outermost layer Au atoms were easily pulled by the chemisorbed species, resulting in the expansion of the outermost layer Au atoms. Nonetheless, it would be subject to more constraints due to the inherent long-range order in the optimized NPG models.

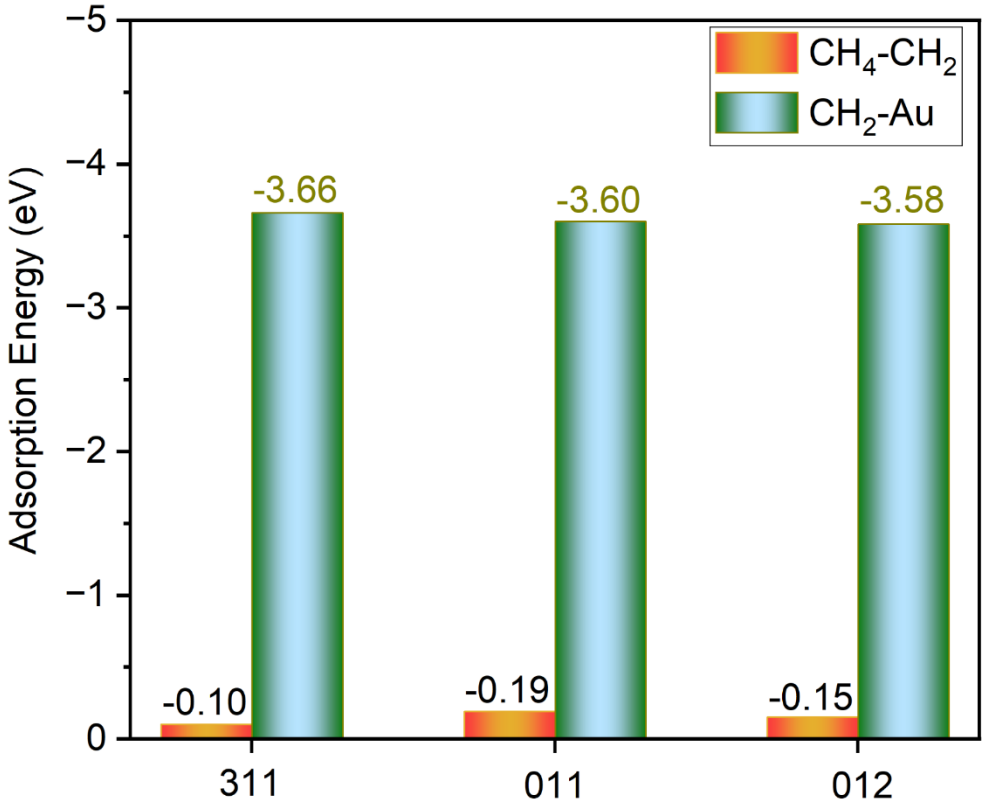

Supplementary Fig. 18 | The adsorption energies of CH_4 on top of $–CH_2$ and $–CH_2$ on different NPG planes. Au{311} corresponds to the adsorption at the edge of Au(111) planes in Fig. 5, Au{011} corresponds to the adsorption at the flat edge of Au(220) planes in Supplementary Fig. 15, and Au{012} corresponds to the adsorption at the stepped edge of Au(220) planes in Supplementary Fig. 16. The relatively low adsorption energies indicate that the interaction between $–CH_2$ and the CH_4 atop is rather weak.

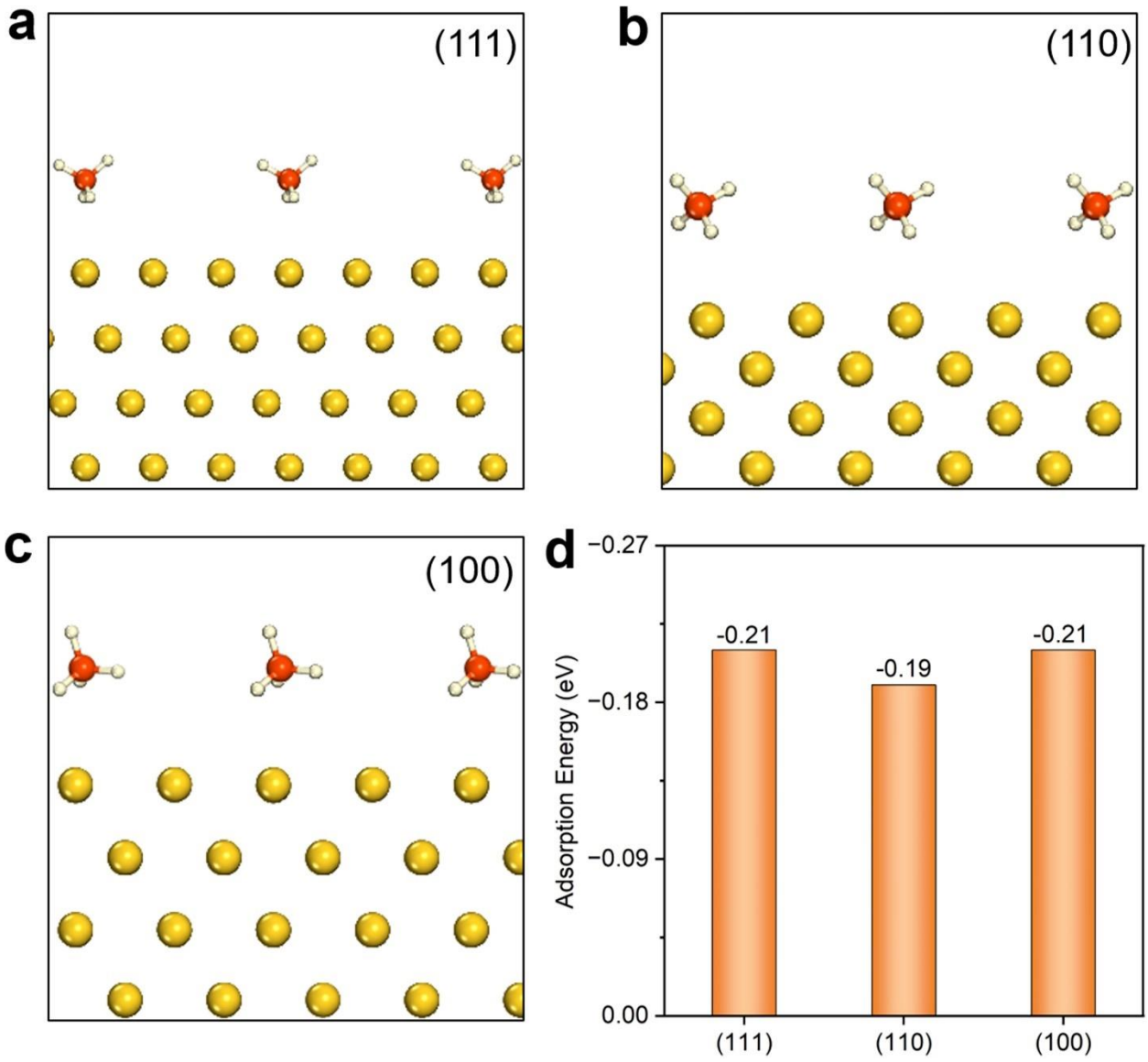

Supplementary Fig. 19 | Adsorption configurations and energies for CH_4 adsorption at different flat surfaces of NPG. a, Au(111), **b,** Au(110), **c,** Au(100), and **d,** adsorption energies.

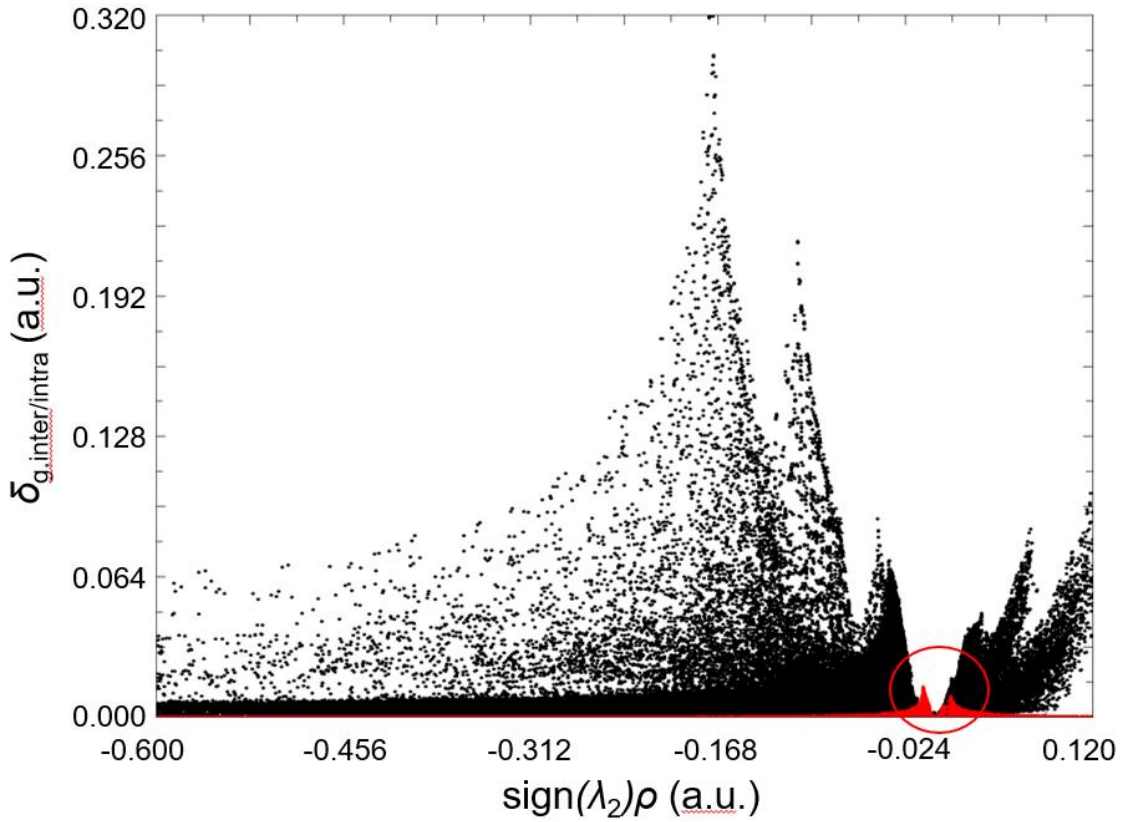

Supplementary Fig. 20 | The interaction analysis between –CH_2 and the CH_4 atop at the edge of Au(111) planes by an IGM method. Black dots present the intra-interaction in fragments, and the red dots correspond to the interaction between fragments.

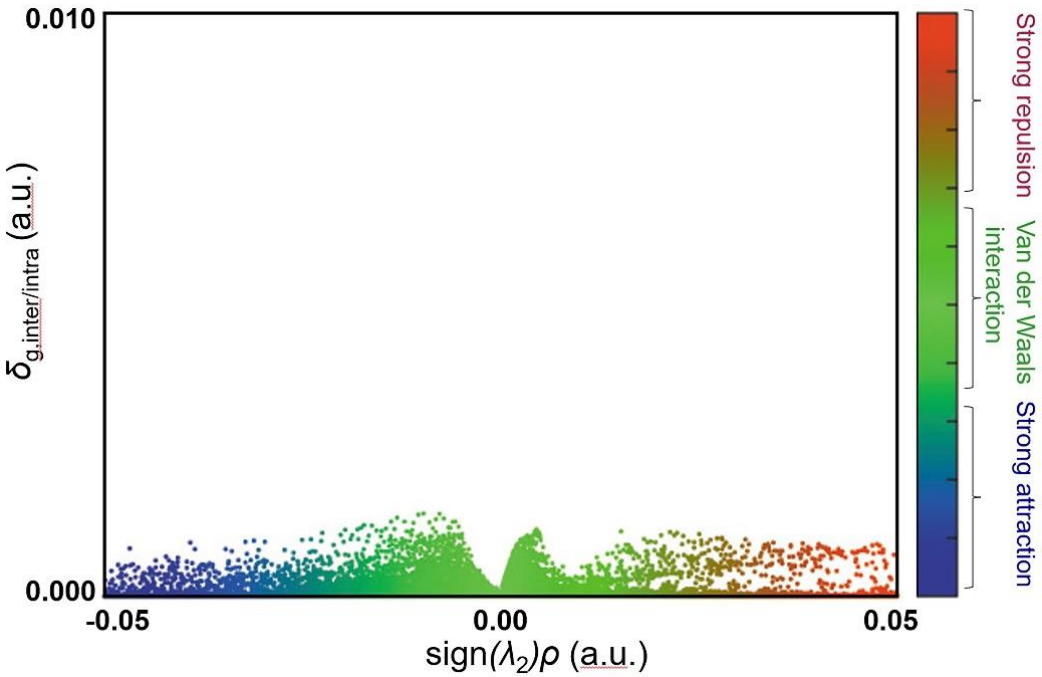

Supplementary Fig. 21 | The interaction analysis between the CH_4 atop and Au(111) planes in the double-layered adsorption structure by an IGM method.

5

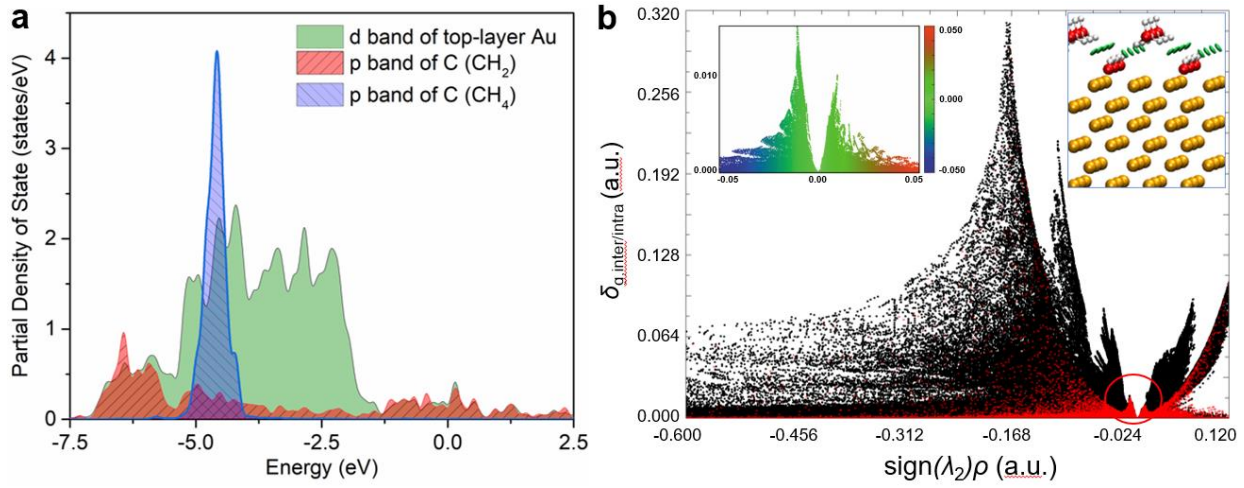

Supplementary Fig. 22 | The interaction analysis between –CH_2 and the CH_4 atop at the flat edge of Au(220) planes by an IGM method. a, Partial density of states analysis corresponding to Supplementary Fig. 15c. **b,** The interaction analysis between –CH_2 and CH_4 at the edge of Au(220) planes by an IGM method; A van der Waals interaction identified. The black dots in (**b**) present the intra-interaction in fragments, and the red dots correspond to the interaction between fragments.

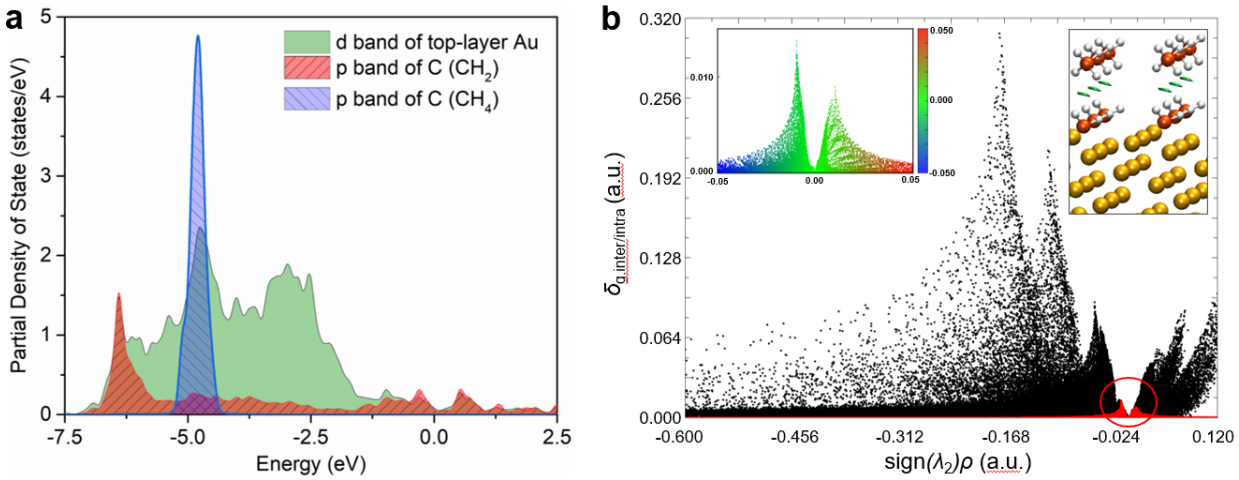

Supplementary Fig. 23 | The interaction analysis between –CH_2 and the CH_4 atop at the periodic stepped edge of Au(220) planes by an IGM method. a, Partial density of states analysis corresponding to Supplementary Fig. 16c. **b,** The interaction analysis between –CH_2 and CH_4 at the edge of the Au(220) planes by an IGM method; A van der Waals interaction was identified. The black dots in (**b**) present the intra-interaction in fragments, and the red dots correspond to the interaction between fragments.

Supplementary Video 1.

The formation process of the reaction intermediate adsorption structures.

Supplementary Video 2.

The entire evolution of the reaction intermediate “crystalline structure” in Fig. 3a.

Supplementary Video 3.

CH_4 dynamically adsorbing on the active –CH_2/NPG ensemble analyzed by AIMD.

Supplementary Video 4.

The dynamic wave-like undulate surface of NPG with the reaction intermediates and products adsorbing on the surface during CH_4 decomposition.

Supplementary Video 5.

The dynamic evolution of the double-layered reaction intermediates.